POLITECNICO DI TORINO
Repository ISTITUZIONALE

Influence of nucleus deformability on cell entry into cylindrical structures

(Article begins on next page)

25 April 2024

Biomechanics and Modeling in Mechanobiology

Influence of nucleus deformability on cell movement into cylindrical structures

--Manuscript Draft--

Influence of nucleus deformability on cell movement into cylindrical structures.

C. Giverso[1] [*], A. Grillo[1], L. Preziosi[1]

[1] Department of Mathematical Sciences, Politecnico di Torino, Corso Duca degli Abruzzi 24, 10129 Torino, Italy

Abstract.
   Mechanical properties of cell nucleus have been demonstrated to play a fundamental role in cell movement across extracellular networks and micro-channels. In this work, we focus on the mathematical description of a cell entering a cylindrical channel composed of extracellular matrix. An energetic approach is derived in order to obtain a necessary condition for which cells enter cylindrical structures. The nucleus of the cell is treated either (i) as an elastic membrane surrounding a liquid droplet or (ii) as an incompressible elastic material with Neo-Hookean constitutive equation. The results obtained highlight the importance of the interplay between mechanical deformability of the nucleus and the capability of the cell to establish adhesive bonds.

Key words: nucleus deformability, cell migration, micro-channel, cell mechanical properties, bond force.

1. Introduction

Cell migration inside extracellular matrix networks plays a critical role in many physiological and pathological processes. For instance, in wound healing the deposition of ECM and the migration of cells through it contribute to repair both epithelial layers and connective tissues, whereas in immune surveillance and inflammation, leukocytes actively migrate towards the site of infection [15]. On the other hand, in pathological conditions, cell migration is involved, for example, in chronic inflammatory diseases and in cancer cell invasion and metastasis formation [42].
Moreover, with the advent of tissue engineering, the process of cell migration is finally exploited

---

[*]Corresponding author. E-mail: chiara.giverso@polito.it

1

in biomedical applications for the regeneration of various tissues, both in vivo and in vitro [4, 59]. From the biological point of view, an increasing number of experimental works has been designed in order to determine cell properties and functions that are involved in the dynamics of motion inside the extracellular microenvironment, and the contribution of this complex network of structural fibrous proteins on the overall process (see, for instance, [20, 32, 40, 56]). In particular, the key factors for cell migration on flat substrates are the dynamic adhesion of cells to their environment via the expression of adhesive molecules (in particular integrins) and the generation of the force necessary for propulsion by contraction of cytoskeletal elements [16]. These are also the basic "ingredients" in the process of migration inside three-dimensional (3D) porous environments. However, in this case, cells require steering their way throughout steric obstacles. This process can be supported by the production of proteolytic enzymes (e.g. Matrix Metalloproteinases, MMPs) able to degrade matrix components in order to open gaps for cell movement [13, 14, 41, 58]. The migratory and invasive process is generally associated with both significant cell deformation and cytoskeletal force generation while passing through constricted openings of the ECM [40, 56].

Indeed cells are exposed to a variety of mechanical stresses and deformations [30], especially, when the proteolytic machinery is inhibited or during migration inside artificial rigid scaffold. Cellular and nuclear deformation require substantial reorganization of the cytoskeleton and compression of the keratin envelope of the nuclear region, in order to acquire an elongated configuration, allowing the entire cell to completely squeeze and stretch (see Fig. 1(a)). Indeed, it has been observed that inside ECM channels, nucleus shape and keratin network structure strongly deviate from the normal spatial distribution in the undeformed cell [40].

These biological findings highlight that the dimensionality of the environment strongly affects cell migratory capabilities and that the deformability of the cell, and in particular of the nucleus, are crucial for cell migration in 3D structures.

The first efforts in describing mechanical behaviour of living cells were aimed at understanding cell response to mechanical stress in the vascular system (e.g., red and white blood cells) [46]. In order to measure the mechanical properties of cells, these must be deformed in some way by a known force or stress and the corresponding deformation must be measured.

In the last years several tests have been developed to pursue this aim. In particular some of the most used mechanical instruments are atomic force microscope (AFM), optical trap (laser tweezers), microcompression method and micropipette suction [23, 24, 34]. Despite the wide range of technological instrument available, the description of mechanical properties of cells is still at a primitive stage and a constitutive theory able to describe cell behaviour is still missing.

Even though the scientific community is becoming aware of the importance of mechanical properties of cells in their process of migration inside porous structures, poor investigations have been carried from the mathematical modelling point of view and mechanical information is generally neglected in the description of cell movements.

Nowadays, if we want to describe the movement of a population of cells inside a region containing extracellular matrix, from the continuum mechanics point of view, Darcy's Law is generally used

$$\boldsymbol{v}_c = -\frac{k(\phi_{ECM})}{\nu(1 - \phi_{ECM})}\nabla P \,.$$

Therefore cells are viewed as a liquid continuum with velocity $\boldsymbol{v}_c$ and dynamic viscosity ν that can flow through the ECM structure, with porosity $\varepsilon = 1 - \phi_{ECM}$ (where ϕ_{ECM} is the volume fraction of the ECM) driven by the gradient of the interstitial pressure, ∇P. The permeability, $k(\phi_{ECM})$, which is a scalar only if the ECM is isotropic (with respect to the flow), is generally a function of porosity (e.g. Kozeny-Carman or Holmes-Mow [25]), but it is often assumed to be a constant [35, 39, 53]. Sometimes the orientation of ECM fibres is considered [5, 6, 36]. However, to our knowledge, mechanical properties of cells are always neglected in the description of cell migration in porous structures.

Even when we move towards the length scale at which discrete models are used, the mechanical properties of cells are poorly considered, unless we move towards really detailed models of the cells. One of them, is the tensegrity model [26, 27], in which loads are supported by struts in compression and cables in tension. Clearly, this description is close to reality, but the high complexity of this model makes it difficult to be used in simulations with a big number of cells and to be up-scaled to the description of macroscopic behaviours.

Some first efforts to include cells mechanical properties inside the description of cell movement on 2D and inside 3D substrates has been done in [44, 45] using Cellular Potts Models (CPM), which allow intuitive representation of cells and their mechanical properties, without requiring too expensive computations.

The introduction of microscopic mechanical properties of cells into continuum macroscopic equations are of fundamental importance in order to make a step towards a more comprehensive representation of cells and tissue. To do that, we study how the nucleus deformability can influence the process of a cell entering a 3D extracellular structure, using a continuum description of the cell nucleus. Even though, in vivo, fibre structures and bundles are arranged into really complex networks of strongly varying local densities [57], that create pores and gaps, we simplify the problem, considering the ECM structured in parallel cylindrical channels composed of fibres and bundles that provide directional guidance cues to cells. This is of course a strong assumption of the far more complex real structure of the extracellular environment, but it can be a good approximation for regular scaffolds used in tissue engineering and moreover it helps to make a first step towards the description of the real phenomenon.

This paper is organized as follows: in Section 2 we review micropipette experiments and the related classical aspiration criteria, commenting the difficulty encountered in applying them to the description of a cell entering an ECM channel. It is shown that these models cannot account for the boundedness of cells and therefore they lead to some unrealistic results (reported in the Appendix). A simple mathematical model for adhesive forces, required to accomplish the process, is analysed in Section 3. In particular, we point out two possible representations of the force that the distribution of bonds can exert (linear vs. constant) and we make some considerations on the extension of the adhesive area (boundedness assumption). In Section 4 we propose a mathematical model, based on an energetic approach, able to describe the deformation of a spherical finite elastic structure (representing the nucleus) into an elongated deformed one, that can move inside the channel. Two different representations for nuclear deformation are implemented (ellipsoidal vs.

BIOLOGICAL
EXPERIMENT

BIOLOGICAL
REPRESENTATION

MATHEMATICAL
REPRESENTATION

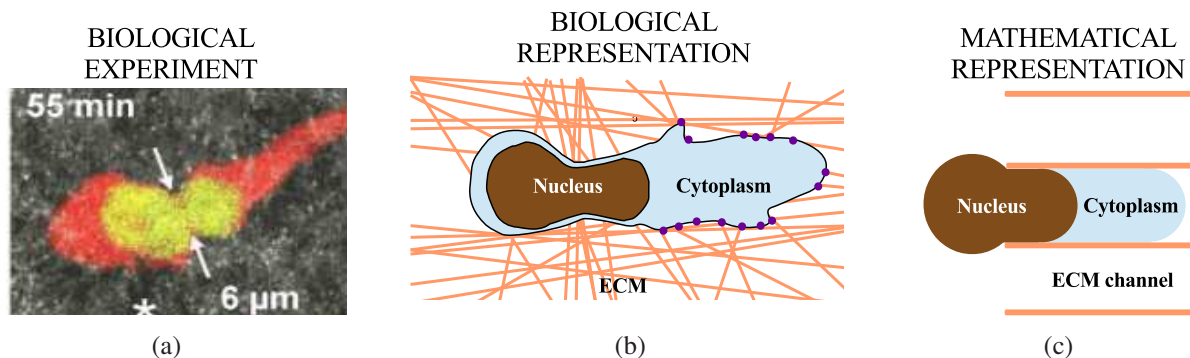(a)   (b)   (c)

Figure 1: Nuclear deformation during cell migration: biological experiments and schematic representation of the process. (a) Confocal time-lapse snapshot of cell migration inside mid-density collagen (3.3 mg/ml) shows nuclear (in green) and cytoplasmic (in red) shape change (with permission from [17]). (b) Biological sketch of the process of cell migrating through 3D matrix of fibres. Dots denote focal contacts, pink lines stand for ECM fibres (adapted from [17]). (c) Schematic representation of the geometry considered in the model: the cytosol (light blue) can freely move into one of the cylindrical channels composed of ECM bundles, whereas the nucleus stands on the back and progressively deforms in order to enter the channel.

cigar-shaped). The nucleus is mechanically assimilated either to an elastic membrane (section 4.1) or to an elastic solid (section 4.2). The computational findings are reported and discussed in Section 5. Results are presented in terms of dimensionless parameters that represent the interplay between adhesive and mechanical properties.

2.   Mathematical Model of Micropipette Aspiration

A cell can be schematically represented as consisting of two main compartments, the cytoplasm and the nucleus, both surrounded by lipid bilayer membranes. The cytoplasm holds all cell's internal sub-structures (except for the nucleus) immersed in what is called cytosol. The cytosol, which fills much of the volume of the cell, is composed by a complex mixture of cytoskeleton filaments, dissolved macro-molecules and water. The nucleus is less deformable than the cytoplasm [17] and its deformability is mainly regulated by both chromatin structure, and lamin intermediate filaments forming a part of the nuclear envelope [17, 18].

When migrating inside a thick 3D fibrous environment made of extracellular matrix, with typical pore sizes smaller than the cellular diameter, cells need to deform both their cellular body and their nucleus. Being the nucleus the stiffest organelle, the nuclear deformability strongly contributes to the migration efficiency of a cell, whereas it is much easier for the cytosol (and the embedded organelles) to extend its protrusion while the nucleus lags behind (see Fig. 1(a)).

In order to describe the above complex environment we simplify the geometry considering the motion of a cell in a cylindrical microchannel as a micropipette. In this respect micropipette aspi-

ration is one of the most common way to study the mechanical behavior of living cells and it can help understanding the process of a cell entering inside a functionalized channel. In the typical experiment, a cell is aspirated into a small glass tube applying a suction pressure. The leading edge of its surface is tracked with light microscopy. It is observed that, if the suction pressure is sufficiently high, both soft cells (e.g., neutrophils, that normally transmigrate across small pores) and more rigid cells (e.g., chondrocytes and endothelial cells) completely enter pipettes, within a certain range of calibers (see [24] for a review). In both cases the response to an aspiration pressure is similar until a hemispherical projection is formed inside the pipette. Beyond that point, for cells behaving like a liquid surrounded by a membrane, a further increase in the suction pressure can cause the complete entry of the cell into the channel [12]. On the other hand, when cells behaving like a solid are aspirated, they do not flow into the micropipette when the aspiration length exceeds the pipette radius, rather the surface extends until a new equilibrium position is reached [28, 49]. Because of the small suction pressures relative to the osmotic pressure of isotonic saline solution in which cells are positioned, in all these experiments cells usually deform at constant volume [24]. Some simple continuum models, treating the cell either as a liquid droplet surrounded by an elastic cortical shell [60], or as a homogeneous elastic membrane [7], or as a solid [49] have been formulated in order to fit experimental data. Even though these models do not consider the high heterogeneity in cell composition, they surprisingly make good predictions of the cell deformation response to known suction forces produced by the pipette and they are still used today in the biomechanical community.

In Evans' model [60], cells are described as passive viscous liquid droplet encapsulated by a distinct cortical layer, with cortical tension, T_c. The equilibrium condition comes directly from Laplace law applied to the suction of a cell until a hemispherical projection is formed inside the pipette. Calling L_p the aspired length and R_p the pipette radius, the critical suction pressure drop ΔP_c is obtained for $L_p/R_p = 1$, when the following relation holds

$$\frac{\Delta P_c R_p}{T_c} = 2\left(1 - \frac{R_p}{R_c}\right) \tag{2.1}$$

where R_c is the radius of the cell outside the pipette (when $L_p/R_p = 1$). The cortical tension creates a threshold pressure drop below which the cell will not enter the pipette and above which cells can flow into it. Moreover Evans et al. [60] observed that the rate at which a cell flows into a pipette is almost constant, with only a small nonlinearity over time until the cell completely enters the pipette.

When the cell has totally entered the pipette all the microscopic "ruffles" and "folds" have been pulled smooth. However they observed there exists a lower limit below which cells cannot enter the pipette, that for the specific cells used in their biological experiments (granulocytes) corresponds to a caliber of $2.7\mu m$ [11, 12].

For what concerns cells behaving like a solid, many studies have been done on human red blood cell. The interior of this anucleate cells is a Newtonian liquid and the biconcave shape comes from its membrane. The deformation of such cells has been studied under a constant area assumption [7, 9, 10, 55], to derive the suction pressure ΔP needed to aspire a portion of cell of length L_p inside a cylindrical channel of radius R_p, which is given by the following relation (that holds for

$L_p > R_p$)

$$\frac{\Delta P R_p}{\gamma} = 2\frac{L_p}{R_p} - 1 + \log\left(2\frac{L_p}{R_p}\right), \tag{2.2}$$

where γ is the shear elastic modulus of the membrane.
Eq. (2.2) is obtained as the stationary condition of the kinematic relation

$$\frac{\Delta P R_p}{\gamma} = 2\frac{L_p}{R_p} - 1 + \log\left(2\frac{L_p}{R_p}\right) + 4\frac{\eta}{\gamma}\frac{\dot{L}_p}{R_p}, \tag{2.3}$$

where a viscoelastic stress-strain relation is assumed for the membrane. Therefore in (2.3) γ represents the elastic properties of the membrane, whereas η its viscosity.
Experimentally it has been observed that, when $\dfrac{L_p}{R_p} > 1$, the relation between $\dfrac{\Delta P R_p}{\gamma}$ and $\dfrac{L_p}{R_p}$ is almost linear, with a slope equal to 2.45. This consideration leads to the well known Chien's relation [7]

$$\frac{\Delta P R_p}{\gamma} = 2.45\frac{L_p}{R_p} \quad \left(\frac{L_p}{R_p} > 1\right). \tag{2.4}$$

Finally, Theret et al. [49] studied the entry into a channel of a cell treated as a homogeneous elastic solid, with Young's modulus equal to E. Their analysis for an infinite, homogeneous half-space drawn into a micropipette can be summarized by the following relation

$$\frac{\Delta P}{E} = \frac{2\pi}{3}\Phi\frac{L_p}{R_p}, \tag{2.5}$$

where Φ is a factor linking the external and internal radius of the pipette, which is assumed to be equal to 2.1 in many works [24].

The process of a cell entering a glass tube has some similarities with the process of a cell entering a channel composed of ECM fibres. Of course in the biological movement of cell migration across matrix channels, we do not have any aspiring pressure, but what makes the cells deform and enter the channel is the capability of cells to form adhesive bonds with the ECM, that actively pull them, through the contraction of filaments composing the cytoskeleton. Therefore, the ΔP in eq. (2.2)-(2.5) should be related to the total adhesive force expressed by cell-ECM bonds, $\pi R_p^2 \Delta P \approx F_{adhesion}^Z$, where $F_{adhesion}^Z$ is the component on the long axis of the cell. We will give more details about these forces in Section 3.
Moreover we can assume that only the nucleus of the cell behaves as an elastic material, applying eq. (2.2)-(2.5) to the deformation of the cellular nucleus only. Even though results obtained under these hypothesis seem promising (see Appendix), we have to be aware that we are pushing the criteria away from their limit of validity. In fact, Chien's and Theret's models have been obtained assuming, respectively, an infinite 2D membrane and a 3D half space aspired inside a pipette. Moreover, the pipettes used in Chien's biological experiments ranged from $0.3\,\mu m$ up to $0.8\,\mu m$ and the volumes aspired into the pipettes were always $< 5\%$ of the cell volume [7]. At the same time, even though the pipettes used by Theret et al. [49] were bigger (with an internal

diameter ranging between 2 μm and 3 μm), the portion of the cell aspired was two-to-four times R_p. Therefore both validations stay away from the complete entry of the cell. Actually, all these studies were designed in order to determine the mechanical properties of cells in the first stages of the deformation and they apply best to problems in which the displacement and their gradient are quite small (normally L_p/R_p up to 5 [49]), whereas micropipette experiments account also for the total aspiration of the cell.

3. Adhesive forces

To describe cell entry into ECM channels, a fundamental step is the definition of adhesive forces, that lead to cell deformation and migration inside the channel. The adhesive force can be thought as the resultant of all forces generated by single cell-ECM bonds on the surface of adhesion through the contraction of the cytoskeleton. Cell-matrix adhesion is mainly mediated by integrins on the cell surface that connect ECM to the cytoskeleton. The adhesion can be modulated by the density of expressed and activated integrins, $\rho_b = N_{integrin}/S_{cell-ECM}$ (where $N_{integrin}$ is the number of integrins over the surface of contact between the cell and the ECM, $S_{cell-ECM}$), and by the density of substratum ligands (ECM adhesive sites), here represented by the ECM surface ratio, $\alpha_{ECM} = S_{ECM}/S_{channel}$. We will assume that the cytoplasm can easily penetrate inside the channel without any constrictions (see Fig. 2), so that the action of adhesive bonds will cause on one hand the translation of the cytosolic region (keeping the same shape with a tip that will be modelled as a spherical cap) and on the other hand the advancement of the nucleus, that, being at the entrance of the microchannel, will deform to penetrate into it. We can approximately say that the length of the region in contact with the channel wall and in front of the nucleus is approximately constant and we can assume that on this surface bonds are formed. Therefore, referring to Fig. 2 and defining $S = \left\{ (X, Y, Z) : X^2 + Y^2 = R_p^2, \, \bar{Z}_{low}(t) < Z < \bar{Z}_{up}(t) \right\}$ the surface for which ECM-bonds are expressed, we can say that the length for which bonds are formed, $L_b = \bar{Z}_{up}(t) - \bar{Z}_{low}(t)$ remains constant in time during cell deformation.

Accepting that the density of bonds on cell surface, ρ_b, and the portion of the channel wall composed of ECM adhesive sites, α_{ECM}, do not depend on time, the total adhesion force is

$$\mathbf{F}_{adhesion} = \int_S \rho_b(\mathbf{X})\alpha_{ECM}(\mathbf{X})\mathbf{F}_{bond}(\mathbf{X})dS, \qquad (3.1)$$

where $\mathbf{F}_{bond}(\mathbf{X})$ is the force generated through cytoskeleton contraction, as a consequence of bond formation. Though ρ_b and α_{ECM} may be generally functions of the space, in the homogeneous case, eq. (3.1) simplifies into

$$\mathbf{F}_{adhesion} = \rho_b\alpha_{ECM} \int_S \mathbf{F}_{bond}(\mathbf{X})dS. \qquad (3.2)$$

The total adhesive force pulling the cell is therefore a function of the radius of the pipette, the density of bonds ρ_b, the surface fraction of the channel composed of extracellular matrix, α_{ECM}, and the integral of the single bond forces over the length of contact. In particular, under the

assumption that the length for which bonds are formed is given by the portion of the cell in front of the nucleus in contact with the channel (see Fig. 2), we have

$$L_b = L_{cell}^0 - R_p - L_n^0 \tag{3.3}$$

where L_{cell}^0 is the initial length of the cell inside the channel (which corresponds to the length of the deformed cytoplasm) and L_n^0 is the portion of the nucleus that can enter the pipette without any deformation. Easy geometrical reasoning, based on volume conservation of both the cytoplasm and the nucleus, gives

$$L_{cell}^0 = R_p \left[\frac{4}{3} \frac{R_c^3 - R_n^3}{R_p^3} + \frac{1}{3} + \frac{1}{R_p^3} \left(L_n^0 \right)^2 \left(R_n - \frac{1}{3} L_n^0 \right) \right] , \tag{3.4}$$

$$L_n^0 = R_n - \sqrt{R_n^2 - R_p^2}, \tag{3.5}$$

where R_p is the radius of the cylindrical channel, R_n the radius of the nucleus and R_c the radius of the cell. Once that a proper function representing bonds forces is provided the process of adhesive force description is accomplished. In particular, we will consider the following simple forms of F_{bond}^Z, which is the Z-component of the bond force that will do the work to accomplish cell penetration in the microchannel.

Linear bond force

We assume that on each bond it is exerted a force proportional to the distance between the nucleus and the site in which the bond is formed, i.e.,

$$F_{bond}^Z = k_b Z , \tag{3.6}$$

where k_b is the elastic constant of the bond. Substituting (3.6) into (3.2) we obtain

$$F_{adhesion}^Z = \pi R_p \rho_b \alpha_{ECM} k_b L_b^2 . \tag{3.7}$$

This relation takes into account the biological observation that the biggest adhesive forces are expressed at the apical portion of the cell [1, 8, 33, 38]. However it has the disadvantage that there is no upper limit to the adhesive force that can be exerted by a bond, which is not true. This may become important when the size of the channel is very small causing long cell extensions (see section 5).

Constant bond force

We assume that a fixed force, $F_{bond}^Z = F_b^M$, is exerted on each cell-ECM bonds, which implies that

$$F_{adhesion}^Z = 2\pi R_p \rho_b \alpha_{ECM} F_b^M L_b . \tag{3.8}$$

This relation represents the fact that there is a mean force that bonds can exert and a maximum force over which bonds break, that has been experimentally measured, [2, 37, 38, 48].
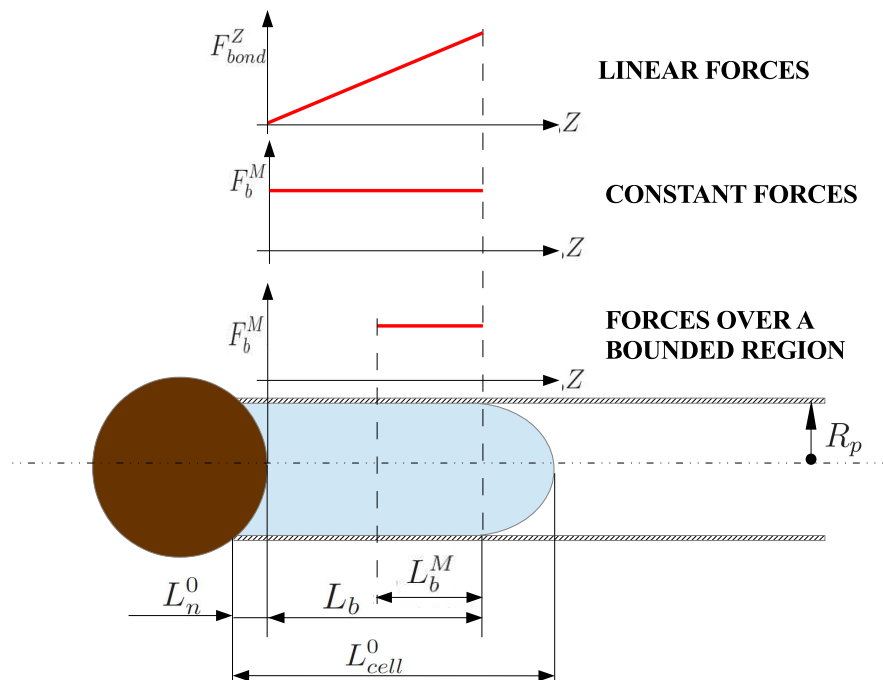
Figure 2: Schematic representation of the length of the adhesive region and of the types of forces considered.

Force over a bounded region

We consider the case in which cells are able to form bonds only over a certain area of the contact region, e.g. the apical portion of the deformed cell. Therefore, taking a constant force assumption, we have $F_{bond}^Z = F_b^M \chi_{L_b^M}(Z)$, where L_b^M represents the length of the maximal area of contact for which bonds are formed (adhesive region) and

$$\chi_{L_b^M}(Z) = \begin{cases} 1 & \text{if} \quad (L_b - L_b^M)_+ < Z < L_b \\ 0 & \text{if} \quad 0 \le Z \le (L_b - L_b^M)_+ \vee Z \ge L_b \end{cases}$$

where $(\cdot)_+$ stands for the positive part of $(\cdot)$, to take into account that for protrusions smaller than L_b^M all the cytoplasmic membrane participates in the adhesion process. Therefore, the total adhesive force is represented by the following relation

$$F_{adhesion}^Z = 2\pi R_p \rho_b \alpha_{ECM} F_b^M L_b^* , \tag{3.9}$$

where $L_b^* = \min\{L_b, L_b^M\}$. This relation prevents adhesive forces to growth dramatically for $R_p \to 0$ and it represents the fact that for very small pipette radius the cell cannot extend his protrusion over too large areas.

A similar relation would be achieved if the interval over Z is substituted by several disconnected intervals. In this case χ is the sum of the sizes of the intervals. Also the localization of these "adhesive sites" does not affect the final result, provided that the overall length is the same.

Analogously, it is possible to use the linear force assumption, taking $F_{bond}^Z = k_b Z \chi_{L_{b,el}^M}(Z)$, that leads to

$$F_{adhesion}^Z = 2\pi R_p \rho_b \alpha_{ECM} k_b L_{b,el}^* \left(L_b - \frac{1}{2} L_{b,el}^* \right) , \tag{3.10}$$

where $L_{b,el}^* = \min\{L_b, L_{b,el}^M\}$. However with a proper re-definition of $L_{b,el}^M$ as a function of L_b^M, eq. (3.10) leads to the same results as (3.9), when $L_b > L_b^M$.

4. Energy Balance Models

We tackle the problem of a cell entering a cylindrical ECM channel using an energetic approach. Always working under constant volume assumption, we develop two models to analyse the total energy required to deform the initial spherical nucleus (see Fig. 3(a)) into a nucleus that is totally inside a cylindrical channel. As observed in [54] the central nucleus acquires an elongated shape when the cell is forced to cross channels of different geometries. Experimental evidences [29, 54] suggest that, when the cell elongates, the initially spherical nucleus significantly deforms, orienting with respect to the cell long-axis direction. Cell elongation is associated with the formation of parallel actin bundles on either sides of the nucleus, that are responsible of the nuclear deformation and help maintaining the deformed configuration. Indeed, during cell elongation, the tension in actin filaments grows and generates compressive forces acting laterally on both sides of the nucleus [54].

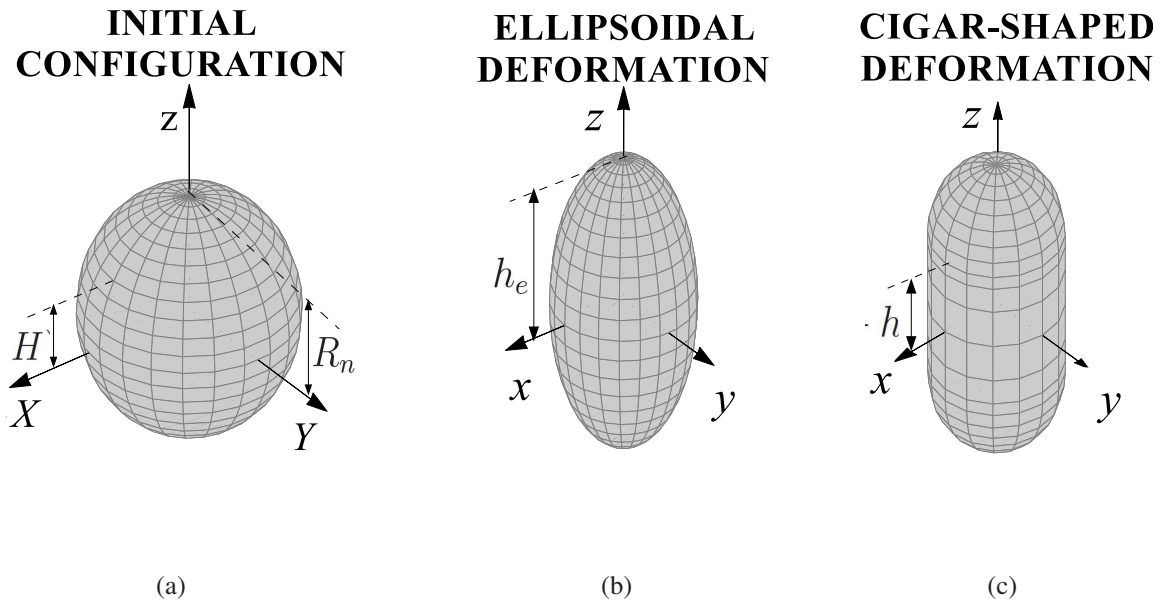The shape of the deformed cell can be approximated either

Figure 3: Deformation from (a) the initial spherical configuration to the final one, considering (b) an ellipsoidal and (c) a cigar-shaped deformed nucleus

- by a prolate ellipsoid [54, 58], with smaller axis R_p (see Fig. 3(b)) or

- by a cigar-like shape (see Fig. 3(c)), with cylindrical central region of radius R_p and hemispherical caps [58].

Concerning the calculation of the energy required to deform the nucleus, we consider the two cases in which:

- all the energy is spent to increase the membrane area of the nucleus, whereas the material inside is treated as an inviscid liquid that freely rearranges following the geometry of the channel (see subsection 4.2);

- all the energy is spent to deform the internal solid nucleus of the cell, treated as an elastic material (see subsection 4.3).

Of course, these hypotheses are one the opposite of the other and intermediate situations should be studied (i.e., energy of membrane plus bulk energy). We recall once again that, in both cases, the cytoplasm can freely move inside the channel.

The energy required to deform the initial spherical shape will then be compared to the work done by adhesion forces, described in section 3, to make the cell advance in the microchannel. We will give more details on the work done by bonds in subsection 4.1.

11

4.1. Bond Energy Model

The work required to have the cell completely inside the channel should be provided by adhesive forces. We can express the adhesive energy as

$$\mathcal{W}_{adhesion} = F^Z_{adhesion} \Delta L \,, \tag{4.1}$$

where ΔL is the total displacement of the cell nucleus inside the channel, and $F^Z_{adhesion}$ is the resultant directed along the Z-axis of all forces exerted by cell-ECM bonds, described in Section 3. In the following we will assume that $\Delta L = L_n^{fin} - L_n^0$, where L_n^{fin} is the final length of the nucleus when it is totally inside the channel and it varies depending on the representation chosen for the deformation of the nucleus. Indeed, for the ellipsoidal shape we have that $L_{n,ellips}^{fin} = 2h_e$, where

$$h_e = \frac{R_n^3}{R_p^2} \tag{4.2}$$

is the longer semi-axis of the prolate ellipsoid that preserves the initial volume, whereas considering the cigar nucleus $L_{n,cigar}^{fin} = 2(h + R_p)$, where h can be easily computed, assuming the conservation of the nuclear volume

$$h = \frac{2}{3} R_p \frac{R_n^3 - R_p^3}{R_p^3} \,. \tag{4.3}$$

On the other hand L_n^0 is the initial length of the nucleus that can freely enter the channel without any deformation and it is given by eq. (3.4).

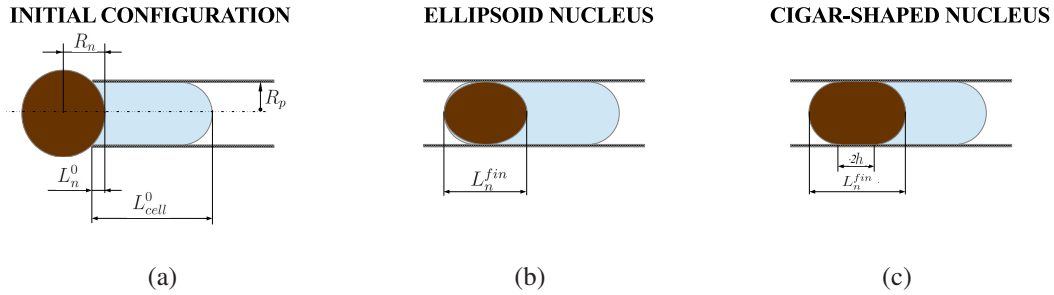Figure 4: Schematic representation of cell displacement and nucleus deformation.

4.2. Membrane Energy Model

As a first example, we consider the case in which the volume of the nucleus is treated as a liquid droplet surrounded by an elastic shell. The energy required to increase the surface area, $\mathcal{W}_{tot}^S$, can be approximated by the following relation [10]

$$\mathcal{W}_{tot}^S = \lambda (\Delta S)^2 \tag{4.4}$$

where ΔS is the increase in the surface area of the cell passing from an initial spherical shape to its final conformation.

We remark that (4.4) has the same form of the term representing surface area increasing in Cellular Potts Models [19].

The increment in the surface area, ΔS, can be easily calculated, assuming that the volume is preserved and computing the new surface area of the deformed nucleus. Using the ellipsoidal deformation assumption, the increment in the surface area is given by

$$
\begin{aligned}
\Delta S_{ellips} & = & S_{ellips} - S_{sphere} = 2\pi R_p^2 \left(1 + \frac{h_e}{R_p e} \sin^{-1}(e)\right) - 4\pi R_n^2 = \\
& = & 4\pi R_n^2 \left[\frac{1}{2}\tilde{R}_p^2 \left(1 + \frac{1}{\tilde{R}_p^3 \sqrt{1 - \tilde{R}_p^6}} \sin^{-1}\left(\sqrt{1 - \tilde{R}_p^6}\right)\right) - 1\right].
\end{aligned}
\tag{4.5}
$$

where $e = \sqrt{1 - \dfrac{R_p^2}{h_e^2}}$ and h_e is given by (4.2) and all distances have been conveniently scaled with the nucleus radius, defining the dimensionless quantity $\tilde{R}_p = R_p/R_n$. Therefore $\dfrac{\mathcal{W}^S}{(4\pi R_n^2)^2}$ is a function of $\tilde{R}_p$. Actually, in the following all the quantities with a tilde represent the corresponding distance scaled with R_n.

On the other hand, using the cigar-shaped deformation hypothesis we have

$$
\begin{aligned}
\Delta S_{cigar} & = & S_{cigar} - S_{sphere} = 4\pi R_p^2 + 2\pi R_p(2h) - 4\pi R_n^2 = \\
& = & 4\pi R_n^2 \left(\frac{1}{3}\tilde{R}_p^2 + \frac{2}{3\tilde{R}_p} - 1\right)
\end{aligned}
\tag{4.6}
$$

where the height of the cylindrical portion of the cigar, $2h$, is given by (4.3).

More complex formulae can be applied to describe the energy required to increase shell area, such as those proposed in [22, 47, 50, 51], however eq. (4.4) can be used to make easy analytical computations and it has been shown to well represent cell behaviour at least in a certain range of deformations [10].

4.3.   Solid Nucleus Model

To compute the energy required to deform the nucleus of the cell treated as a simple solid, we have to assume a proper constitutive equation, representing the response of the material to deformations, and calculate the deformation gradient, $\mathbb{F}$.

Nowadays, a representation of Cauchy stress tensor of cellular components is still under investigation. For sake of simplicity, we assume an incompressible neo-Hookean constitutive law for the nucleus of the cell, therefore the elastic stored energy per unit volume is given by

$$
\mathcal{W}^V = \frac{\mu}{2}\left[\text{tr}(\overline{\mathbb{C}}) - 3\right],
\tag{4.7}
$$

where $\overline{\mathbb{C}} = J^{-2/3}\mathbb{F}^T\mathbb{F}$, $J = \det(\mathbb{F})$ and μ is the shear modulus of the nucleus.

In both the cases in which the deformed nucleus has an ellipsoidal shape and the case in which it acquires a cigar-shaped conformation, we assume that parallel planes perpendicular to the axis of the cylinder in the undeformed configuration, $Z = \text{const}$, are mapped into parallel planes in the final deformed geometry, $z = \text{const}$. Using the standard notation of continuum mechanics, capital letters refers to quantities in the initial configuration whereas lower cases refer to quantities in the deformed configuration. Therefore with (X, Y, Z) we indicate the cartesian coordinates in the undeformed configuration and with (x, y, z) the corresponding cartesian spatial coordinates. Sometimes cylindrical coordinates are used, denoted with (ρ, Φ, Z) and with (r, ϕ, z) in the undeformed and deformed configuration, respectively. The calculation shown in the following are based on merely geometrical considerations.

4.3.1. Ellissoidal deformed nucleus

The deformation of a sphere in a prolate ellipsoid with the same volume is simply given by a uniaxial deformation

$$\mathbb{F} = \text{diag}\left\{\frac{R_p}{R_n}, \frac{R_p}{R_n}, \frac{R_n^2}{R_p^2}\right\} = \text{diag}\left\{\tilde{R}_p, \tilde{R}_p, \frac{1}{\tilde{R}_p^2}\right\}. \tag{4.8}$$

For the particular $\mathbb{F}$ given by (4.8), we can rewrite eq. (4.7) as

$$\mathcal{W}^V = \frac{\mu}{2}\left(2\tilde{R}_p^2 + \frac{1}{\tilde{R}_p^4} - 3\right), \tag{4.9}$$

which integrated over the total volume of the initial sphere gives the total energy required to pass from the initial to the final configuration, i.e.,

$$\mathcal{W}_{tot}^V = \int_{V_r} \mathcal{W}^V \, dV = \frac{2}{3}\mu\pi R_n^3\left(2\tilde{R}_p^2 + \frac{1}{\tilde{R}_p^4} - 3\right), \tag{4.10}$$

where V_r is the volume of the cell in the reference configuration.

Eq. (4.10) links the elastic energy of deformation to the mechanical properties of the nucleus, μ, the morphological properties of the nucleus R_n and the radius of the channel, R_p.

4.3.2. Cigar-shaped nucleus

Another slightly different possibility is that the solid sphere (representing the nucleus), deforms into a cigar-shaped nucleus, composed of a cylinder of radius $\tilde{R}_p$ and height $\tilde{h} = \dfrac{h}{R_n}$ and two hemispherical caps (see Fig. 3(c)).

In order to obtain the deformation gradient we subdivide the initial spherical nucleus into three

regions: the central one, of scaled height $\tilde{H} = \dfrac{H}{R_n}$, is mapped into the cylindrical portion of dimensionless radius $\tilde{R}_p$ and scaled height $\tilde{h}$ defined by (4.3), whereas the upper and lower poles of the nucleus are mapped into the apical and basal hemispheres of the cigar-shaped nucleus. Therefore the deformation gradient can be described as

$$\mathbb{F} = \begin{cases} \mathbb{F}_{N-pole} & \text{for} \quad \tilde{H} \le Z \le 1 \,; \\ \mathbb{F}_c & \text{for} \quad -\tilde{H} < Z < \tilde{H} \,; \\ \mathbb{F}_{S-pole} & \text{for} \quad -1 \le Z \le -\tilde{H} \,. \end{cases} \tag{4.11}$$

Assuming symmetry, we can restrict our analysis to the upper half of the nucleus, i.e. $0 \le Z \le 1$. To derive the deformation gradient of the central region, $\mathbb{F}_c$, we consider a reference slice of height ε and volume $V_r(\varepsilon)$, which is mapped into the final volume $V_f(\varepsilon)$. Assuming that the volume is conserved and passing to the infinitesimal limit, we obtain

$$1 = \lim_{\varepsilon \to 0} \frac{V_f(\varepsilon)}{V_r(\varepsilon)} = \lim_{\varepsilon \to 0} \frac{\pi \tilde{R}_p^2 \left(z(Z + \varepsilon) - z(Z)\right)}{\pi \left(1 - Z^2\right)\varepsilon - \pi \left(Z\varepsilon^2 + \dfrac{\varepsilon^3}{3}\right)} = \frac{\tilde{R}_p^2}{1 - Z^2}\frac{\partial z}{\partial Z} \,, \tag{4.12}$$

which leads to

$$\frac{\partial z}{\partial Z} = \frac{1 - Z^2}{\tilde{R}_p^2} \,. \tag{4.13}$$

We assume that all the slices of the reference "barrel" remain parallel while deforming, i.e $\dfrac{\partial z}{\partial Z}$ is constant for all the points belonging to the same plane parallel to the XY-plane. We then consider an internal volume of the reference spherical region of height ε and volume $V_r(\varepsilon) = \pi\rho^2\varepsilon + o(\varepsilon)$ (for $\varepsilon \to 0$), which is deformed into a volume $V_f = \pi r^2 \left(z(Z + \varepsilon) - z(Z)\right)$. Keeping in mind the relation (4.13) we obtain

$$r = \frac{\rho}{\sqrt{1 - Z^2}}\tilde{R}_p \,. \tag{4.14}$$

Assuming that $\phi = \Phi$, for the central volume of the sphere, one then has the following matrix representation of the deformation gradient in normalized bases of cylindrical coordinates (for both configurations)

$$\mathbb{F}_c = \begin{bmatrix} \dfrac{\tilde{R}_p}{\sqrt{1 - Z^2}} & 0 & \dfrac{\tilde{R}_p Z \rho}{(1 - Z^2)^{3/2}} \\ 0 & \dfrac{\tilde{R}_p}{\sqrt{1 - Z^2}} & 0 \\ 0 & 0 & \dfrac{1 - Z^2}{\tilde{R}_p^2} \end{bmatrix} \,. \tag{4.15}$$

To fulfil the problem of describing the total deformation gradient, we have to consider the upper and lower portion of the sphere, which are mapped into the two hemispheres of the cigar-shaped

nucleus. Considering a slice in these region, in analogy with the central region, we have the following zZ-component of the deformation gradient

$$\frac{\partial z}{\partial Z} = \frac{1 - Z^2}{\tilde{R}_p^2 - (z - \tilde{h})^2} \,. \tag{4.16}$$

We remark that (4.16) holds for $\tilde{H} \leq Z \leq 1$ and $\tilde{h} \leq z \leq \tilde{h} + \tilde{R}_p$.
Also in this case, assuming that undeformed parallel planes remain parallel in the deformed configuration, we obtain

$$r = \frac{\sqrt{\tilde{R}_p^2 - (z - \tilde{h})^2}}{\sqrt{1 - Z^2}} \rho \,, \tag{4.17}$$

that coupled with the hypothesis $\phi = \Phi$ gives the following deformation gradient in cylindrical coordinates, for the upper pole of the sphere

$$\mathbb{F}_{N-pole} = \begin{bmatrix} \dfrac{\sqrt{\tilde{R}_p^2 - (z - \tilde{h})^2}}{\sqrt{1 - Z^2}} & 0 & \Gamma(Z)\rho \\[4mm] 0 & \dfrac{\sqrt{\tilde{R}_p^2 - (z - \tilde{h})^2}}{\sqrt{1 - Z^2}} & 0 \\[4mm] 0 & 0 & \dfrac{1 - Z^2}{\tilde{R}_p^2 - (z - \tilde{h})^2} \end{bmatrix} , \tag{4.18}$$

where

$$\Gamma(Z) = \left(\frac{Z\sqrt{\tilde{R}_p^2 - (z - \tilde{h})^2}}{(1 - Z^2)^{3/2}} - \frac{(z - \tilde{h})\sqrt{1 - Z^2}}{\left(\tilde{R}_p^2 - (z - \tilde{h})^2\right)^{3/2}} \right) \,.$$

We observe that, for the particular form of $\mathbb{F}_c$ and $\mathbb{F}_{N-pole}$ the deformation gradient, $\mathbb{F}$ is continuous.
In order to express all the quantities in the material frame, we integrate eq. (4.16), which gives the implicit relation between the eulerian coordinate z and the corresponding material one, Z

$$(z - \tilde{h})^3 - 3\tilde{R}_p^2(z - \tilde{h}) + 3(Z - \tilde{H}) - (Z^3 - \tilde{H}^3) = 0 \,. \tag{4.19}$$

Eq. (4.19) is a cubic function in z and it has three real solutions, but only the root

$$z(Z) = \tilde{h} + 2\tilde{R}_p \cos\left[\frac{1}{3}\cos^{-1}\left(\frac{(Z - \tilde{H})(Z^2 + \tilde{H}^2 + Z\tilde{H} - 3)}{2\tilde{R}_p^3}\right) + \frac{4}{3}\pi\right] \tag{4.20}$$

is acceptable and can be substituted in (4.18) to have the deformation gradient in terms of the Lagrangian coordinates.
Eq. (4.19) can also be used to derive $\tilde{H}$, given $\tilde{h}$. Indeed substituting $z = \tilde{h} + \tilde{R}_p$, with $\tilde{h}$ given by

eq. (4.3), and $Z = 1$ in (4.19) we have a cubic function of the new unknown $\tilde{H}$, which gives as the only acceptable solution

$$\tilde{H} = 2\cos\left[\frac{1}{3}\cos^{-1}\left(\tilde{R}_p^3 - 1\right) + \frac{4}{3}\pi\right] . \tag{4.21}$$

As for the ellipsoidal deformation, once that the deformation gradient is known it is possible to compute the total energy required to pass from the initial configuration to the final configuration. Still assuming an incompressible neo-Hookean constitutive law (4.7) for the nucleus of the cell, the elastic energy stored per unit volume in the central portion of the sphere is

$$\mathcal{W}_c^V = \frac{\mu}{2}\left[2\frac{\tilde{R}_p^2}{1 - Z^2} + \frac{\tilde{R}_p^2 Z^2 \rho^2}{(1 - Z^2)^3} + \frac{(1 - Z^2)^2}{\tilde{R}_p^4} - 3\right] , \tag{4.22}$$

whereas the energy for the upper and lower poles of the spheres is

$$
\mathcal{W}_{N-pole}^V = \mathcal{W}_{S-pole}^V = \frac{\mu}{2}\left[2\frac{\tilde{R}_p^2 - (z - \tilde{h})^2}{1 - Z^2}\right] +
$$
$$
+ \frac{\mu}{2}\left[\left(\frac{Z\sqrt{\tilde{R}_p^2 - (z - \tilde{h})^2}}{(1 - Z^2)^{3/2}} + \frac{(z - \tilde{h})\sqrt{1 - Z^2}}{\left(\tilde{R}_p^2 - (z - \tilde{h})^2\right)^{3/2}}\right)^2 \rho^2\right] +
$$
$$
+ \frac{\mu}{2}\left[\frac{(1 - Z^2)^2}{\left(\tilde{R}_p^2 - (z - \tilde{h})^2\right)^2} - 3\right] , \tag{4.23}
$$

where $z = z(Z)$ is given by (4.20). To obtain the total energy required to pass from the initial spherical configuration to the cell totally deformed inside the channel, we have to integrate over the corresponding domains in which the deformation is experienced, i.e.,

$$
\mathcal{W}_{tot}^V = \int_{V_r^c} \mathcal{W}_c^V dV + \int_{V_r^{N-pole}} \mathcal{W}_{N-pole}^V dV + \int_{V_r^{S-pole}} \mathcal{W}_{S-pole}^V dV =
$$
$$
= 2\left(\int_{V_r^{c+}} \mathcal{W}^V dV + \int_{V_r^{N-pole}} \mathcal{W}_{N-pole}^V dV\right) , \tag{4.24}
$$

where V_r^c is the volume of the central zone in the reference configuration, V_r^{N-pole} and V_r^{S-pole} are the volume of the north and south pole of the sphere and V_r^{c+} is the volume of the upper-half central part of the sphere, i.e.,

$$V_r^{c+} = \left\{(\rho, \Theta, Z) \in \mathbb{R}^3 : 0 \le \rho \le \sqrt{1 - Z^2}, 0 < \Theta \le 2\pi, 0 \le Z < \tilde{H}\right\} ,$$

whereas

$$V_r^{N-pole} = \left\{(\rho, \Theta, Z) \in \mathbb{R}^3 : 0 \le \rho \le \sqrt{1 - Z^2}, 0 < \Theta \le 2\pi, \tilde{H} \le Z \le 1\right\} ,$$

17

The previous integral can be easily computed in the central region

$$
\begin{aligned}
\mathcal{W}_c^{tot} \;=\; & \mu\pi R_n^3 \left[2\tilde{R}_p^2\tilde{H} + \frac{1}{2}\tilde{R}_p^2 \left(\tanh^{-1}\tilde{H} - \tilde{H} \right) \right] + \\
+ \;& \mu\pi R_n^3 \left[\frac{1}{\tilde{R}_p^4} \left(\tilde{H} - \tilde{H}^3 + \frac{3}{5}\tilde{H}^5 - \frac{1}{7}\tilde{H}^7 \right) - 3 \left(\tilde{H} - \frac{\tilde{H}^3}{3} \right) \right] .
\end{aligned}
\tag{4.25}
$$

We observe that since $\tilde{H}$ is a function of $\tilde{R}_p$ through (4.21), $\dfrac{\mathcal{W}_c^{tot}}{\mu R_n^3}$ is a function of $\tilde{R}_p$.

On the other hand, for what concerns $\int_{V_r^{N-pole}} \mathcal{W}_{N-pole}^V dV$, using the fact that the domain of integration is normal with respect to the XY-plane, we can express the triple integral as a simple integral

$$
\begin{aligned}
\mathcal{W}_{N-pole}^{tot} \;=\; & \frac{\pi\mu}{2}R_n^3 \left[2\int_{\tilde{H}}^1 \left[\tilde{R}_p^2 - (z-\tilde{h})^2 \right] dZ \right] + \\
+ \;& \frac{\pi\mu}{2}R_n^3 \left[\frac{1}{2}\int_{\tilde{H}}^1 \left(\frac{Z\sqrt{\tilde{R}_p^2-(z-\tilde{h})^2}}{(1-Z^2)^{3/2}} + \frac{(z-\tilde{h})\sqrt{1-Z^2}}{\left(\tilde{R}_p^2-(z-\tilde{h})^2\right)^{3/2}} \right)^2 \left(1-Z^2\right)^2 dZ \right] + \\
+ \;& \frac{\pi\mu}{2}R_n^3 \left[\int_{\tilde{H}}^1 \frac{(1-Z^2)^3}{\left(\tilde{R}_p^2-(z-\tilde{h})^2\right)^2} dZ - 2 + \left(2+\tilde{R}_p^2\right)\sqrt{1-\tilde{R}_p^2} \right] ,
\end{aligned}
\tag{4.26}
$$

that needs to be evaluated numerically, in order to obtain an estimate of the total energy required to deform the nucleus.

5.   Results

In this subsection we present the results obtained with the energy balance model, presented in section 4. When the elastic membrane model (subsection 4.2) is used, we consider that the cell can enter the channel if

$$
\mathcal{W}_{adhesion} \geq \mathcal{W}_{tot}^S ,
\tag{5.1}
$$

where $\mathcal{W}_{adhesion}$ is given by (4.1) and $\mathcal{W}_{tot}^S$ has the form presented in eq. (4.4). On the other hand, when the elastic solid nucleus model (subsection 4.3) is applied, the nucleus can enter the cylindrical structure if

$$
\mathcal{W}_{adhesion} \geq \mathcal{W}_{tot}^V ,
\tag{5.2}
$$

where $\mathcal{W}_{tot}^V$ has the form presented in either eq. (4.10) for the ellipsoidal deformation or eq. (4.24) for the cigar-shaped one. Depending on the hypothesis used to describe adhesive bonds (linear

vs. constant vs. bounded) and the geometry chosen for the deformed nucleus (ellipsoid vs. cigar-shaped), inequalities (5.1) and (5.2) lead to the results presented in Table 1, with respect to the diameter ratio $\tilde{R}_p$. $\tilde{L}_b^{(*)}$ stands either for $\tilde{L}_b = L_b/R_n$ in the case of the constant force assumption or $\tilde{L}_b^* = L_b^*/R_n$ for the bounded adhesive region case. By scaling all distances with R_n and writing all material parameters on the right-hand-side, we identify four dimensionless numbers that represent the ratio between adhesive bond properties and nuclear mechanical parameters. In particular, for the elastic membrane model we name

$$G_\lambda^k \; = \; \frac{\rho_b \alpha_{ECM} k_b}{\lambda} \qquad \text{and} \qquad G_\lambda^F \; = \; \frac{\rho_b \alpha_{ECM} F_b^M / R_n}{\lambda} \, ,$$

whereas, when the elastic nucleus model is used, we introduce

$$G_\mu^k \; = \; \frac{\rho_b \alpha_{ECM} k_b R_n}{\mu} \qquad \text{and} \qquad G_\mu^F \; = \; \frac{\rho_b \alpha_{ECM} F_b^M}{\mu} \, .$$

At the numerator we have all the parameters that characterize bonds forces (densities of bonds, surface ratio of ECM, elasticity of bonds or maximum force that bonds can exert) whereas at the denominator we have the parameter describing the mechanical properties of the cell nucleus (λ in the case of an elastic membrane, μ in the case of an elastic solid).
In Table 1,

$$\mathcal{I}(\tilde{R}_p) \; = \; \frac{\mathcal{W}_c^{tot}}{\frac{4}{3}\pi\mu R_n^3} + 2\frac{\mathcal{W}_{N-pole}^{tot}}{\frac{4}{3}\pi\mu R_n^3} \, .$$

The right-hand-side of each relation identifies the critical value of the characteristic number and it is indicated in the following with $\overline{G}_i^j$ (with $i = \{\lambda, \mu\}$, $j = \{k, F\}$). Therefore, once a proper model is chosen, for every diameter ratio $\tilde{R}_p$, it is possible to define the value of $\overline{G}_i^j$, above which a cell, with a nucleus of dimension R_n can enter a channel of radius $\tilde{R}_p R_n$.
We remark that this model, taking into account the finiteness of the nuclear dimensions, is valid only for $\tilde{R}_p \leq 1$. Indeed, when $\tilde{R}_p \to 1$, the elastic energy required to deform the nucleus is almost null, whereas, allowing the cytoskeleton to enter the channel, the adhesive energy is not null and it can easily pull the nucleus inside the channel.

Fig. 5 shows the value of (a) $\overline{G}_\lambda^k$ in the case of linear forces, (b) $\overline{G}_\lambda^F$ in the case of constant forces and (c) $\overline{G}_\lambda^F$ for constant force over a bounded adhesive region, above which the cell can enter a channel of scaled radius $\tilde{R}_p$, when the elastic membrane model is used. On the other hand, Fig. 6 reports the ratios (a) $\overline{G}_\mu^k$ and (b-c) $\overline{G}_\mu^F$ obtained applying the elastic nucleus model, under the same hypothesis of adhesive forces.
Both in Fig. 5 and 6 solid lines represent ellipsoidal deformations, whereas dashed lines stand for cigar-shaped final configurations. In any case, the assumption on the geometry acquired by the deformed nucleus does not affect the qualitative behaviour of the solutions.
We remark that in Fig. 5(a) and (b), for very small radius, the energy required to increase the area of the nuclear membrane increases but the energy exerted by bonds increases faster and therefore,

Table 1: Energy based criteria

Model		Linear Force	Constant (bounded) Force
Elastic membrane	Ellipsoid	$G_\lambda^k \geq 16\pi \dfrac{\left[\frac{1}{2}\tilde{R}_p^2\left(1+\frac{\sin^{-1}(e)}{\tilde{R}_p^3 e}\right)-1\right]^2}{\tilde{R}_p \tilde{L}_b^2 \Delta \tilde{L}_{ellips}}$	$G_\lambda^F \geq 8\pi \dfrac{\left[\frac{1}{2}\tilde{R}_p^2\left(1+\frac{\sin^{-1}(e)}{\tilde{R}_p^3 e}\right)-1\right]^2}{\tilde{R}_p \tilde{L}_b^{(*)} \Delta \tilde{L}_{ellips}}$
	Cigar	$G_\lambda^k \geq 16\pi \dfrac{\left(\frac{1}{3}\tilde{R}_p^2+\frac{2}{3\tilde{R}_p}-1\right)^2}{\tilde{R}_p \tilde{L}_b^2 \Delta \tilde{L}_{cigar}}$	$G_\lambda^F \geq 8\pi \dfrac{\left(\frac{1}{3}\tilde{R}_p^2+\frac{2}{3\tilde{R}_p}-1\right)^2}{\tilde{R}_p \tilde{L}_b^{(*)} \Delta \tilde{L}_{cigar}}$
Elastic nucleus	Ellipsoid	$G_\mu^k \geq \dfrac{2}{3}\dfrac{2\tilde{R}_p^2+\frac{1}{\tilde{R}_p^4}-3}{\tilde{R}_p \tilde{L}_b^2 \Delta \tilde{L}_{ellips}}$	$G_\mu^F \geq \dfrac{2}{3}\dfrac{2\tilde{R}_p^2+\frac{1}{\tilde{R}_p^4}-3}{\tilde{R}_p \tilde{L}_b^{(*)} \Delta \tilde{L}_{ellips}}$
	Cigar	$G_\mu^k \geq \dfrac{4}{3}\dfrac{\mathcal{I}(\tilde{R}_p)}{\tilde{R}_p \tilde{L}_b^2 \Delta \tilde{L}_{cigar}}$	$G_\mu^F \geq \dfrac{2}{3}\dfrac{\mathcal{I}(\tilde{R}_p)}{\tilde{R}_p \tilde{L}_b^{(*)} \Delta \tilde{L}_{cigar}}$

for $\tilde{R}_p \to 0$, the critical G_λ^k and G_λ^F go to zero when the unbounded L_b is used, giving rise to the contradiction that cell can enter pipettes of very small diameters.

Indeed, when the radius of the channel is small, the length of the cytoplasm inside it grows considerably, leading, in the linear case, to adhesive forces that are unrealistically high. In particular, for $\tilde{R}_p \to 0$, we have that the energy required to deform the elastic membrane increases as $\tilde{R}_p^{-3}$, whereas $\Delta L = \mathcal{O}\left(\tilde{R}_p^{-2}\right)$ and $L_b = \mathcal{O}\left(\tilde{R}_p^{-2}\right)$. Therefore, when the linear force assumption is used, $\overline{G}_\lambda^k = \mathcal{O}\left(\tilde{R}_p^3\right)$ for $\tilde{R}_p \to 0$, whereas, when the bond force is assumed constant, $\overline{G}_\lambda^F = \mathcal{O}\left(\tilde{R}_p\right)$ for $\tilde{R}_p \to 0$. In order to avoid the unphysical result, we more realistically assume that bonds are formed on the surface of the channel until the maximum length, L_b^M is reached. Restricting the extent for which bonds are formed to a certain length ($L_b = L_b^*$), will dramatically limit the growth of adhesive energy for very small $\tilde{R}_p$. In this case, for $\tilde{R}_p \to 0$, $L_b = \mathcal{O}(1)$ and thus the critical G_λ^F goes to infinity like $\tilde{R}_p^{-1}$ (see Fig. 5(c)).

The same unrealistic result is obtained using the linear force model coupled with the elastic solid nucleus model (see Fig. 6(a)). In this case, for very small radii, the energy required to deform the elastic nucleus grows as $\tilde{R}_p^{-4}$ and hence, under the linear force assumption, the critical G_μ^k goes linearly for $\tilde{R}_p \to 0$. On the other hand, when a constant force assumption is used, we have that $\overline{G}_\mu^F$ goes to infinity as $\tilde{R}_p^{-1}$, whereas limiting the adhesive region, it goes like $\tilde{R}_p^{-3}$, for $\tilde{R}_p \to 0$.

Fig. 6(b) reports the results obtained applying the elastic solid nucleus model with the constant force assumption, whereas Fig. 6(c) is obtained under the boundedness assumption. In both cases the relation between $\overline{G}_\mu^F$ and $\tilde{R}_p$ is a bijection. Therefore, for every $\tilde{R}_p$ it is possible to uniquely define a minimum value of G_μ^F above which the nucleus is pulled inside the channel, conversely knowing nuclear mechanical and adhesive properties, the minimum value of R_p that allows the nucleus of radius R_n to enter the channel, is determined. Being the discrepancy between results obtained assuming the cigar-shaped and the ellipsoidal deformation very small, it is possible to use
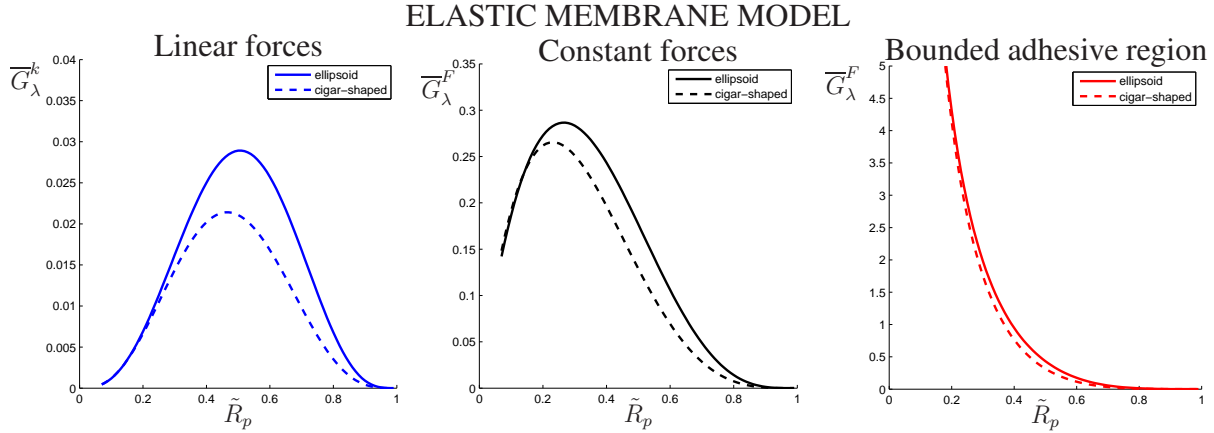
Figure 5: Elastic membrane model: (a) $\overline{G}_\lambda^k$ (in the case of linear forces), $\overline{G}_\lambda^F$ in the case of constant forces (b) and in the case of constant forces over a bounded region, with $\tilde{L}_b^M = 5$ (c). The curves indicate the minimum value of the characteristic numbers that need to be overcome in order to have the cell enter a channel of radius $\tilde{R}_p$.

the analytical relation obtained for the ellipsoidal case

$$\overline{G}_\mu^F = \frac{2}{3} \frac{\left[2\tilde{R}_p^2 + \dfrac{1}{\tilde{R}_p^4} - 3 \right]}{\tilde{R}_p \tilde{L}_b^{(*)} \Delta\tilde{L}_{ellips}} \, . \tag{5.3}$$

Being G_μ^F the ratio between adhesive and mechanical properties, eq. (5.3) shows that with respect to cells with softer nuclei, in order to enter the same channel, more rigid cells (greater μ) should either increase the number of adhesive bonds (ρ_b) or the number of focal points in contact with ECM (α_{ECM}) or even bond strength (F_b^M). This finding is in qualitative agreement with a number of experimental works, such as [3, 40, 56], where cell migratory capability is associated with nuclear deformations and the existence of critical channel radius above which cell can enter has been observed. Moreover it is comparable with the results obtained with discrete model [44, 45], confirming that mechanical properties of the nucleus can affect the cell entry into channels.
Eq. (5.3) can be of great value, for instance, in scaffold design. Indeed, assuming that cell mechanical properties and their capabilities to express bonds are known it is possible to evaluate the pore size that allows the cells to penetrate the rigid network.

6.   Conclusions

Due to the increasingly recognized importance of cell migration process in extracellular matrix environments and its exploitations, e.g., in tissue engineering, theoretical models, able to analyse
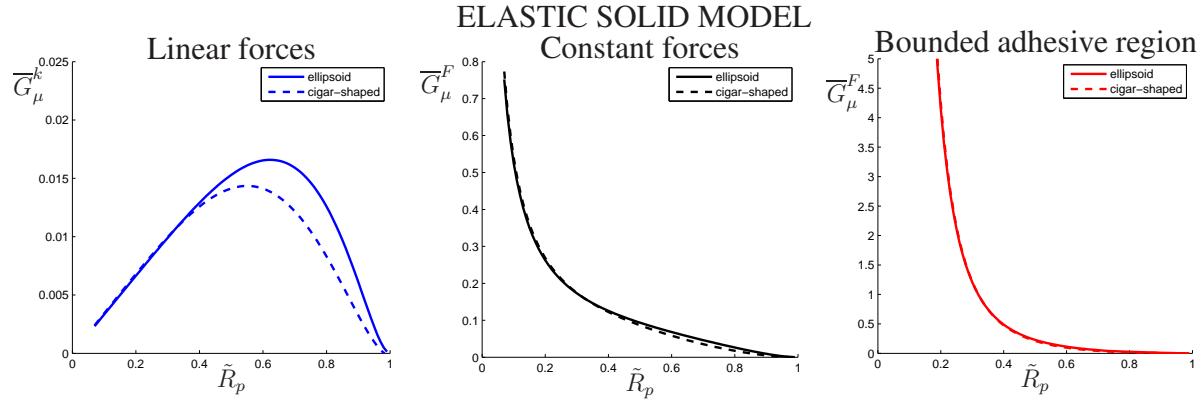
Figure 6: Elastic solid nucleus model: (a) $\overline{G}_\mu^k$ in the case of linear forces, (b) $\overline{G}_\mu^F$ in the case of constant forces and (c) $\overline{G}_\mu^F$ in the case of constant forces over a bounded region (with $\tilde{L}_b^M = 5$), above which the cell can enter a channel of radius $\tilde{R}_p$.

the relative influence of single and interrelated parameters on the overall migratory process, are needed.

We identified some energy-based criteria that take into account the mechanical properties of cell nucleus, the adhesive characteristics of cell membrane, the finiteness of the nucleus and the aspect ratio of the structures involved in cell migration, trying to maintain the model as simple as possible in order to obtain easily manageable results.

For the examples presented, some analytical results are obtained, providing the relation between adhesive and mechanical properties that should be satisfied in order to have cells entering a channel of given radius. Therefore, if adhesive and mechanical properties of the cell are known, it is possible to derive the minimum channel size and, conversely, observing experimentally the capability of a cell to enter cylindrical channels of different dimensions, it is possible to characterize the interplay between mechanical and adhesive properties of cells.

Results show that cells are able to enter ECM-networks only for pore radii bigger than a critical one, depending on the stiffness of the nucleus of the cell and their capabilities to express adhesion molecules in order to bind to the extracellular matrix. Indeed, a rigid cell body would nullify any attempt of the cell to squeeze through channels and network gaps narrower than the nucleus dimension, as observed in [40, 56] .

However, in order to obtain reliable quantitative results, more studies are required, both from the biological and from the mathematical point of view. In particular, more experiments are needed in order to characterize cell mechanical response and a proper relation for the force exerted by adhesive bonds. A more comprehensive understanding on the microscopical mechanism regulating nucleus deformation and cytoscheletal reorganization, when the cell is anchored to ECM, can also help to obtain a more realistic description of the process. Indeed, it has been observed that one of the major determinants of cell rigidity is the filamentous cytoskeleton. In particular, microtubules seem to be implicated in cell shape changes and migration, whereas actin filaments are generally considered more important for elastic resistance to deformation [29].

Moreover, biological experiments are necessary to validate the model presented, once the mechanical characterization of cells is accomplished.

From the mathematical point of view, the model can be improved in several directions in order to reproduce more closely the behavior of cells. For instance, in our ongoing work we want to study the whole dynamic process, considering all the steps of the cell entering the channel. Indeed, the model we proposed is based on an "integral" approach, i.e., it considers the total work required to pass from the initial to the final configuration and, thus, it gives an estimate of the "mean" adhesive forces required, scaled by the mechanical deformability of the nucleus. However, this method does not take into account the possible existence of intermediate states in which the force exerted by bounds should be greater than the force needed to squeeze the nucleus inside the channel. That is, the integral criterion used here to obtain analytical expressions gives a necessary but not sufficient condition for the passage of the cell inside the channel. Therefore a criterion able to establish the maximum force needed would be more precise, though it requires 3D time-dependent numerical simulations.

Of course, one could use more realistic constitutive models representing cell response to stress (hopefully supported by experimental tests) and more complex relations for the force exerted by adhesive bonds. In order to obtain a model able to reproduce more closely the behaviour of cells, in particular, it seems very promising to study the active component that characterizes living matter response to external stimuli.

In spite of all possible developments, the energetic framework presented here is quite general and continues to be valid even for more complex cell and membrane constitutive assumptions. Finally the approach described here could be applied to the design of synthetic scaffolds, with optimal values of pore size and fibre density, that may accelerate cell transport and in-growth, critical for regenerative treatments.

Appendix

Micropipette models applied to cell migration inside channels

For sake of completeness, we consider here the case in which nucleus entry obeys the classical relations (2.2) or (2.5), deforming the initial spherical nucleus into a cigar-like shape, with the assumption that L_p in (2.2) and (2.5) represents the length of the deformed nucleus, i.e. $L_p = L_{n,cigar}^{fin} = 2(h + R_p)$ with h given by eq. (4.3). We define the critical pressure as the value of ΔP for which $L_p = L_{n,cigar}^{fin}$ and we assume that a proper representation for ΔP in eq. (2.2) and (2.5) is $\dfrac{F_{adhesion}^Z}{\pi R_p^2}$, where $F_{adhesion}^Z$ is the Z-component of the adhesive force given either by eq. (3.7) or (3.8) or (3.9). Then, assuming that a pressure above the critical one makes the cell move inside the pipette, it is possible to obtain the relation between mechanical and adhesive parameters that should hold in order to have the cell enter the channel, depending on the geometrical properties (i.e. R_n, R_c and R_p).
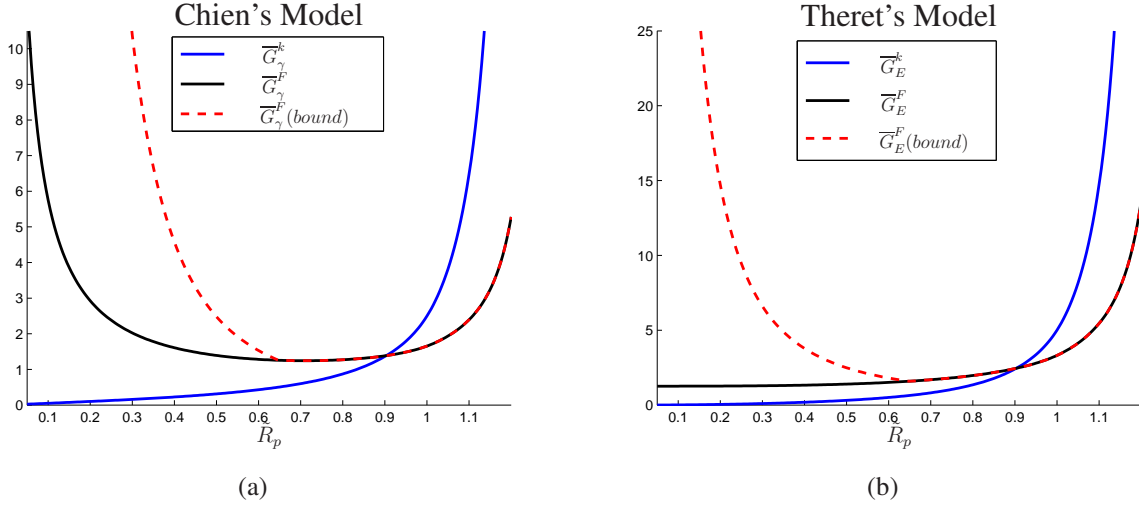
23

(a)   (b)

Figure 7: Critical value of the characteristic numbers obtained applying (a) Chien's model and (b) Theret's model, under either a linear force (blue) or a constant force (black) or a constant force over a bounded region (red dashed) assumption.

The inequalities that should be satisfied in each case are summarized in Table 2, as a function of the diameter ratio $\tilde{R}_p = \dfrac{R_p}{R_n}$. On the left-hand-side of each relation we have characteristic parameters representing the ratio between adhesive properties and mechanical properties of cell nucleus. In particular, we identify

$$G_\gamma^k = \frac{\rho_b \alpha_{ECM} k_b R_n^2}{\gamma}, \quad G_\gamma^F = \frac{\rho_b \alpha_{ECM} F_b^M R_n}{\gamma},$$

$$G_E^k = \frac{\rho_b \alpha_{ECM} k_b R_n}{E}, \quad G_E^F = \frac{\rho_b \alpha_{ECM} F_b^M}{E}.$$

Table 2: Entry criteria

Model	Linear Force	Constant (bounded) Force
Chien	$G_\gamma^k \geq \dfrac{2\dfrac{\tilde{L}_p}{\tilde{R}_p} - 1 + \log\left(2\dfrac{\tilde{L}_p}{\tilde{R}_p}\right)}{\tilde{L}_b^2}$	$G_\gamma^F \geq \dfrac{2\dfrac{\tilde{L}_p}{\tilde{R}_p} - 1 + \log\left(2\dfrac{\tilde{L}_p}{\tilde{R}_p}\right)}{2\tilde{L}_b^{(*)}}$
Theret	$G_E^k \geq \dfrac{2\pi}{3}\Phi\dfrac{\tilde{L}_p}{\tilde{L}_b^2}$	$G_E^F \geq \dfrac{2\pi}{3}\Phi\dfrac{\tilde{L}_p}{2\tilde{L}_b^{(*)}}$

On the right-hand-side of each relation we have the critical value of the characteristic number (indicated with $\overline{G}_i^j$, with with $i = \{\gamma, E\}$, $j = \{k, F\}$), which is a function of the diameter ratio,

being

$$\tilde{L}_p = \frac{L_p}{R_n} = \frac{2}{3}\tilde{R}_p \left[1 + 2\left(\frac{1}{\tilde{R}_p}\right)^3\right] \, ,$$

$$\tilde{L}_b = \frac{L_b}{R_n} = \tilde{R}_p \left[\frac{4}{3}\left(\frac{\tilde{R}_c}{\tilde{R}_p}\right)^3 - \frac{1}{\tilde{R}_p^3} + \frac{1}{3} + \frac{\left(\tilde{L}_n^0\right)^2}{\tilde{R}_p^3}\left(1 - \frac{1}{3}\tilde{L}_n^0\right)\right]$$

with $\tilde{L}_n^0 = 1 - \sqrt{1 - \tilde{R}_p^2}$ and $\tilde{R}_c = R_c/R_n$.

The critical characteristic numbers are plotted in Fig. 7 as a function of the diameter ratio of the channel. The graphs represent the minimum value that each constant should assume in order to have the cell totally inside the channel, according to Chien's criterion (Fig. 7(a)) and Theret's one (Fig. 7(b)). Results obtained with the linearized Chien's equation (2.4) are comparable with the ones obtained with the more complex formula (2.2). In Fig. 7 the dashed line represents results obtained using constant forces over a bounded domain (where we set $\tilde{L}_b^M = 5$). It is possible to see that for big $\tilde{R}_p$, $\overline{G}_\gamma^F$ and $\overline{G}_E^F$ are obviously not influenced by the assumption on the boundedness of the contact region in which integrins are expressed (i.e., the red-dashed curve and the black-solid one overlap). Indeed, it exists an $\tilde{R}_p^*$ such that $L_b^* = L_b$ for $\tilde{R}_p \geq \tilde{R}_p^*$, whereas $L_b^* = L_b^M$ for $\tilde{R}_p < \tilde{R}_p^*$. Therefore the adhesive energy is influenced by the boundedness assumption only for $\tilde{R}_p < \tilde{R}_p^*$.

For instance, Fig. 8 explains how these graphs can be interpreted (for the particular case of Chien model): the bar charts below the graph represent the range of $\tilde{R}_p$ for which a cell characterized by a given G_γ^k or a given G_γ^F can enter the channel.

In the figure, 'cell 1' (orange) is characterized by higher G_γ^k or G_γ^F than 'cell 2' (violet). This means that we are considering either a softer cell (i.e., small γ) or a cell that is able to establish a higher number (i.e., higher $\rho_b \alpha_{ECM}$) of stronger (i.e., bigger k_b or F_b^M) adhesive bonds. In any case, the range for which 'cell 1' can enter the pipette is bigger than for 'cell 2' (orange bars vs. violet bars), according to what we expect from biological observations. Moreover, using the constant force assumption it is possible to see that the range for which cells can enter the pipette is bounded both from below and from above. On the other hand, using the linear force assumption, we do not have any inferior limit, in contrast with biological observation. This contradictory result is due to the hypothesis used in the representation of forces. Indeed in this case the more the cytoplasm of the cell spread inside the channel (small $\tilde{R}_p$), the more bonds can pull the nucleus inside. In particular, even though the force required to deform the nucleus grows as $\tilde{R}_p^{-3}$, as $\tilde{R}_p \to 0$, the bond force raises faster, since $\tilde{L}_b^2 = \mathcal{O}\left(\tilde{R}_p^{-4}\right)$. On the other hand, when a constant force assumption is used, for small $\tilde{R}_p$, the length for which bonds are formed augments $\left(\tilde{L}_b = \mathcal{O}\left(\tilde{R}_p^{-2}\right) \text{ for } \tilde{R}_p \to 0\right)$. Thus, the total force exerted by bonds increases, but it is not sufficient to compensate the greater deformation required to the nucleus, which goes like $\tilde{R}_p^{-3}$ for $\tilde{R}_p \to 0$. Conversely, introducing the boundedness assumption on L_b, the force exerted by bonds is limited.

In particular, we have that for $\tilde{R}_p \to 0$, $\overline{G}_F^\gamma$ goes like $\tilde{R}_p^{-\alpha}$ (with $\alpha = 1$ for unbounded L_b and
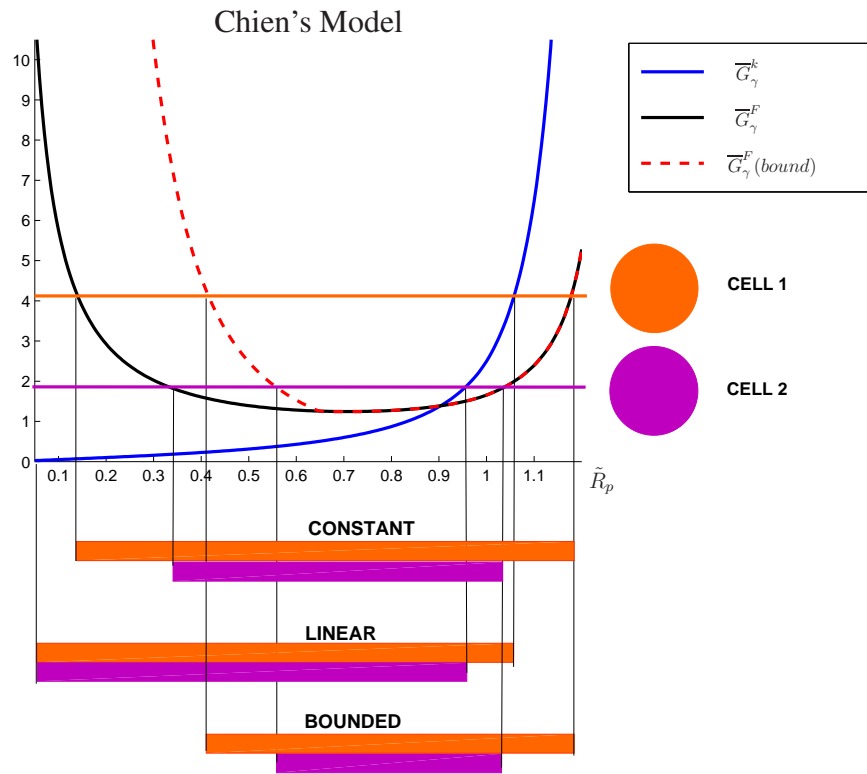
Figure 8: Interpretation of the results: bar charts represents the range for which a cell, with a given G_γ^k or G_γ^F can enter the channel, for the different hypothesis of bond forces.

$\alpha = 3$ when the adhesive region is limited) and $\overline{G}_K^\gamma$ grows linearly.

On the other hand, when the radius of the pipette is very big, the entry of the cell into the channel is limited due to the decrease in the contact area between the cell and the channel wall, where adhesive bonds are formed. It is likely that, in this case, the force exerted by adhesive bonds is not equal to the maximum executable force. Thus, a linear force can better describe the physiological behaviour. Therefore, a good choice for the bond force relation could be a ramp force on a bounded adhesive region, which is also the most conservative case.

In Theret's model it is possible to see that, for $\tilde{R}_p \to 0$, $\overline{G}_E^k = \mathcal{O}\left(\tilde{R}_p^2\right)$ and $\overline{G}_E^F = \mathcal{O}\left(1\right)$ when the constant force assumption with unbounded adhesive region is implemented. Thus neither the constant force assumption nor the linear force one can account for the inferior limit in pipette calibers. Only enforcing the boundedness of the adhesive region, the capability of cells to enter very small channels is prevented.

Both Chien's and Theret's models, with the assumption of adhesive constant forces over a bounded region, provide evidence for a biphasic cell migratory behavior that reveals most optimal migration at pore sizes at nuclear and subnuclear diameters and diminishes at gaps greatly bigger or smaller than the cell nucleus diameter.

However, even though results obtained applying the classical models above seem promising, especially when adhesion is active on a bounded domain, they cannot account for the finite boundaries of the nucleus. Indeed Chien's model refers to an infinite 2D membrane, whereas Theret's one was derived for a 3D half space aspired inside a pipette, only for a small portion. Therefore these criteria cannot be applied to describe the total entry of the cell into a pipette. The consequence of this assumption are evident in Fig. 7, where, for $\tilde{R}_p = 1$, the force needed to deform the nucleus does not vanish.

References

[1] D. Ambrosi, A. Duperray, V. Peschetola, C. Verdier. *Traction patterns of tumor cells.* J. Math. Biol. 58: 163-181 (2009).

[2] W. Baumgartner, P. Hinterdorfer, W. Ness, A. Raab, D. Vestweber, H. Schindler, D. Drenckhahn. *Cadherin interaction probed by atomic force microscopy.* Proc. Nat. Acad. Sci. USA 97: 4005-4010 (2000).

[3] C. Beadle, M.C. Assanah, P. Monzo, R. Vallee, S.S. Rosenfeld, P. Canoll. *The role of myosin II in glioma invasion of the brain*. Mol. Biol. Cell. 19: 3357-3368 (2008).

[4] R.M. Capito, M. Spector. *Scaffold-based articular cartilage repair*. IEEE Eng. Med. Biol. Mag. 22: 42-50 (2003) .

[5] A. Chauvière, T. Hillen, L. Preziosi. *Modeling the motion of a cell population in the extracellular matrix*. Discr. Cont. Dyn. Sys. (Supplements), Special Issue: 250-259 (2007).

[6] A. Chauvière, T. Hillen, L. Preziosi. *Modeling cell movement in anisotropic and heterogeneous network tissues*. Netw. Heterog. Media 2(2): 333-357, (2007).

[7] S. Chien, K.L.P. Sung, R. Skalak, S. Usami, A.C. Usami. *Theoretical and experimental studies on viscoelastic properties of erythrocyte membrane*. Biophys. J. 24: 463-487 (1978).

[8] M. Dembo, Y.L. Wang. *Stresses at the cell-to-substrate interface during locomotion of fibroblasts.* Biophys. J. 76(4): 2307-2316 (1999).

[9] E.A. Evans. *New membrane concept applied to the analysis of fluid shear and micropipette-deformed red blood cells.* Biophys. J. 13: 941-954 (1973).

[10] E.A. Evans, R. Waugh, L. Melnik *Elastic area compressibility modulus of red cell membrane.* Biophys. J. 16: 585-595 (1976).

[11] E.A. Evans, B. Kukan. *Passive material behavior of granulocytes based on large deformations and recovery after deformation tests.* Blood. 64: 1028-1035 (1984).

[12] E.A. Evans, A. Yeung. *Apparent viscosity and cortical tension of blood granulocytes determined by micropipet aspiration.* Biophys. J. 56:151-160 (1989).

[13] P. Friedl, E.B. Brocker. *The biology of cell locomotion within three-dimensional extracellular matrix.* Cell. Mol. Life Sci. 57 (1): 41-64 (2000).

[14] P. Friedl, K. Wolf. *Tumour-cell invasion and migration: diversity and escape mechanisms.* Nat. Rev. Cancer. 3 (5): 362-374 (2003).

[15] P. Friedl, B. Weigelin. *Interstitial leukocyte migration and immune function.* Nat Immunol. 9 (9): 960-969 (2008).

[16] P. Friedl, K. Wolf. *Proteolytic interstitial cell migration: a five-step process.* Cancer Metastasis Rev. 28 (1-2): 129-135 (2009).

[17] P. Friedl, K. Wolf, J. Lammerding. *Nuclear mechanics during cell migration.* Curr. Opin. Cell. Biol. 23 (1): 55-64 (2011).

[18] G. Gerlitz, M. Bustin. *The role of chromatin structure in cell migration.* Trends Cell. Biol. 21 (1): 6-11 (2011).

[19] F. Graner, J. A. Glazier. *Simulation of biological cell sorting using a two-dimensional extended potts model.* Phys. Rev. Let. 69: 2013-2016 (1992).

[20] J. Guck, F. Lautenschläger, S. Paschke, M. Beil. *Critical review: cellular mechanobiology and amoeboid migration.* Integr. Biol. 2: 575-583 (2010).

[21] B.A.C. Harley, H. Kim, M.H. Zaman, I.V. Yannas, D.A. Lauffenburger, L.J. Gibson. *Microarchitecture of three-dimensional scaffolds influences cell migration behavior via junction interactions*. Biophys J. 95 (8): 4013-4024 (2008).

[22] W. Helfrick. *Elastic properties of lipid bilayers: theory and possible experiments*. Z. Natur-forsch. 28 c: 693-703 (1973).

[23] R.M. Hochmuth. *Measuring the mechanical properties of individual human blood cells*. J Biomech Eng. 115(4B): 515-519 (1993)

[24] R.M. Hochmuth. *Micropipette aspiration of living cells*. J. Biomech. 33: 15-22 (2000).

[25] M.H. Holmes, V. C. Mow. *The nonlinear characteristics of soft gels and hydrated connective tissues in ultrafiltration*. J. Biomech. 23(11): 1145-1156 (1990).

[26] D.E. Ingber. *Cellular tensegrity: defining new rules of biological design that govern the cytoskeleton*. J. Cell Sci. 104: 613-627 (1993).

[27] D.E. Ingber. *Tensegrity I. Cell structure and hierarchical systems biology*. J. Cell Science. 116 (7): 1157-1173 (2003).

[28] W.R. Jones, H.P. Ting-Beall, G.M. Lee, S.S. Kelley, R.M. Hochmuth, F. Guilak. *Alterations in the Young's modulus and volumetric properties of chondrocytes isolated from normal and osteoarthritic human cartilage*. J. Biomech. 32(2): 119-127 (1999).

[29] T.P. Kole, Y. Tseng, I. Jiang, J.L. Katz, D. Wirtz. *Intracellular mechanics of migrating brob-lasts*. Mol. Biol. Cell. 16: 328-338 (2005)

[30] S. Kumar, V.M. Weaver. *Mechanics, malignancy, and metastasis: The force journey of a tumor cell*. Cancer Metastasis Rev. 28: 113-127 (2009).

[31] R.M. Kuntz, W.M. Saltzman. *Neutrophil motility in extracellular matrix gels: mesh size and adhesion affect speed of migration*. Biophys. J. 72 (3): 1472-1480 (1997).

[32] F. Lautenschläger, S. Paschke, S. Schinkinger, A. Bruel, M. Beil, J. Guck. *The regulatory role of cell mechanics for migration of differentiating myeloid cells*. Proc. Nat. Acad. Sci. USA 106 (37): 15696-15701 (2009).

[33] W.R. Legant, J.S. Miller, B.L. Blakely, D.M. Cohen, G.M. Genin, C.S. Chen. *Measurement of mechanical tractions exerted by cells in three-dimensional matrices*. Nat. Methods. 7(12): 969-971 (2010).

[34] K. Liu. *Deformation behaviour of soft particles: a review*. J. Phys. D: Appl. Phys. 39: 189 - 199 (2006).

[35] J.S Lowengrub, H.B Frieboes, F. Jin, Y.L Chuang, X. Li, P. Macklin, S.M. Wise, V. Cristini. *Nonlinear modelling of cancer: bridging the gap between cells and tumours*. Nonlinearity. 23: R1-R91 (2010).

[36] K.J. Painter. *Modelling cell migration strategies in the extracellular matrix*. J. Math. Biol. 58: 511-543 (2009).

[37] P. Panorchan, M.S. Thompson, K.J. Davis, Y. Tseng, K. Konstantopoulos, D. Wirtz. *Single-molecule analysis of cadherin-mediated cell-cell adhesion*. J. Cell Sci. 119: 66-74 (2006).

[38] V. Peschetola, V. Laurent, A. Duperray, R. Michel, D. Ambrosi, L. Preziosi, C. Verdier. *Time-dependent traction force microscopy for cancer cells as a measure of invasiveness*. [submitted]

[39] L. Preziosi, G. Vitale. *Mechanical aspects of tumour growth: Multiphase modelling, adhesion, and evolving natural configurations*, in M. Ben Amar, A. Goriely, M. M. Mller, L. F. Cugliandolo, Eds., New Trends in the Physics and Mechanics of Biological Systems, Lecture Notes of the Les Houches Summer School, 92: 177-228, Oxford University Press (2011).

[40] C.G. Rolli, T. Seufferlein, R. Kemkemer, J.P. Spatz. *Impact of tumor cell cytoskeleton organization on invasiveness and migration: A microchannel-based approach*. PLos ONE. 5 (1): e8726 (2010).

[41] F. Sabeh, R. Shimizu-Hirota, S.J. Weiss. *Protease-dependent versus -independent cancer cell invasion programs: three-dimensional amoeboid movement revisited*. J. Cell. Biol. 185 (1): 11-19 (2009).

[42] E. Sahai. *Illuminating the metastatic process*. Nat. Rev. Cancer. 7 (10): 737-749 (2007).

[43] G.W. Schmid-Schonbein, Y. Y. Shih, S. Chien. *Morphometry of human leukocytes*. Blood. 56: 866-875 (1980).

[44] M. Scianna, L. Preziosi, K. Wolf. *A cellular potts model: simulating cell-and extracellular matrix-derived determinants for cell migration on and in matrix environments*. Math. Biosci. Eng. [in press].

[45] M. Scianna, L. Preziosi. *Modelling the influence of nucleus elasticity on cell invasion in fiber networks and microchannels*. [submitted]

[46] R. Skalak. *Modelling the mechanical behavior of red blood cells*. Biorheology. 19: 229-238 (1973).

[47] R. Skalak, A. Tozeren, R.P. Zarda, S. Chien. *Strain energy function of red blood cell membrane*. Biophys. J. 13: 245-264 (1973).

[48] M. Sun, J. Graham, B. Hegedus, F. Marga, Y. Zhang, G. Forgacs, M. Grandbois. *Multiple membrane tethers probed by atomic force microscopy*. Biophys. J. **89**, 4320-4329 (2005)

[49] D.P. Theret, M.L. Lvesque, M. Sato, R.M. Nerem, L.T. Wheeler. *The application of a homogeneous half-space model in the analysis of endothelial cell micropipette measurements*. J. Biomech. Eng. 110: 190-199 (1988).

[50] Z.C. Tu, Z.C. Ou-Yang. *Geometric theory on the elasticity of bio-membranes*. J. Phys. A: Math. Gen. 37: 11407-11429 (2004).

[51] Z.C. Tu, Z.C. Ou-Yang. *Elastic theory of low-dimensional continua and its applications in bio- and nano-structures*. J. Comput. Theor. Nanosci. 5: 422-448 (2008).

[52] N.H. Valerius, O. Stendahl, J.H. Hardwig, T.P. Stossel. *Distribution of actin-binding protein and myosin in polymorphonuclear leukocytes during locomotion and phagocytosis.* Cell. 24: 195-202 (1981).

[53] C. Verdier, J. Etienne, A. Duperray, L. Preziosi. *Review: Rheological properties of biological materials*. C. R. Phys. 10(8): 790-811 (2009).

[54] M. Versaevel, T. Grevesse, S. Gabriele. *Spatial coordination between cell and nuclear shape within micropatterned endothelial cells*. Nature Comm. 3 (2012). doi:10.1038/ncomms1668

[55] R. Waugh, E.A. Evans. *Thermoelasticity of red blood cell membrane*. Biophys. J. 26: 115-132 (1979).

[56] K. Wolf, Y.I. Wu, Y. Liu, J. Geiger, E. Tam, C. Overall, M.S. Stack, P. Friedl. *Multi-step peri-cellular proteolysis controls the transition from individual to collective cancer cell invasion*. Nat. Cell. Biol. 9: 893-904 (2007).

[57] K. Wolf, S. Alexander, V. Schacht, L.M Coussens, U.H von Andrian, J. van Rheenen, E. Deryugina, P. Friedl. *Collagen-based cell migration models in vitro and in vivo*. Semin. Cell. Dev. Biol. 20 (8): 931-941 (2009).

[58] K. Wolf, P. Friedl. *Extracellular matrix determinants of proteolytic and non-proteolytic cell migration*. Trends. Cell. Biol. 21 (12): 736-744 (2011).

[59] I.V. Yannas, E. Lee, D.P. Orgill, E.M. Skrabut, G.F. Murphy. *Synthesis and characterization of a model extracellular matrix that induces partial regeneration of adult mammalian skin*. Proc. Natl. Acad. Sci. USA 86: 933-937 (1989).

[60] A. Yeung, E. Evans. *Cortical shell-liquid core model for passive flow of liquid-like spherical cells into micropipets*. Biophys. J. 56:139-149 (1989).